World Electric Vehicle Journal

MDPI

Article

Sensitivity Screening and Parameter Optimization-Based VCU Calibration Method for Hybrid Electric Vehicles

Jiaqi Qi [1], Liwen Zhang [1], Zhenwei Wang [1,*], Yanqiu Xiao [2], Junjian Hou [1] and Yudong Zhong [1]

[1] Henan Provincial Key Laboratory of Intelligent Manufacturing of High-End Equipment, Zhengzhou University of Light Industry, Zhengzhou 450002, China
[2] Henan Provincial Discipline Construction Research Center, Zhengzhou University of Light Industry, Zhengzhou 450002, China
* Correspondence: 2024034@zzuli.edu.cn

Abstract

VCU parameter calibration is an important means of improving the fuel economy of planetary power-split hybrid electric vehicles, shortening the development cycle, and reducing development and calibration costs. However, conventional VCU parameter calibration methods still suffer from strong dependence on engineering experience, inadequate parameter screening, and insufficient optimization robustness. To address these issues, an optimization-based VCU calibration method is proposed for a planetary power-split hybrid electric system. First, based on the architecture of the planetary power-split hybrid electric system and its rule-based energy management strategy, the state-of-charge (SOC) threshold, power demand threshold, and charging coefficient are selected as the initial calibration parameters. Their feasible ranges are then determined according to the allowable battery SOC operating window, vehicle power demand distribution, and SOC balance constraints. Subsequently, theoretical combined fuel consumption per 100 km is adopted as the system response, and both local and global sensitivity analyses are conducted to identify the key calibration parameters and quantify their interaction effects. Finally, an adaptive simulated annealing algorithm is introduced to perform global optimization of the key parameters and obtain the optimal VCU parameter combination. The simulation results indicate that the power demand threshold and SOC threshold are the dominant factors affecting combined fuel consumption. After optimization, the SOC threshold is reduced from 72% to 55%, while the power demand threshold is reduced from 27 kW to 7 kW. Consequently, the theoretical combined fuel consumption decreases from 16.71 L/100 km to 15.97 L/100 km, corresponding to a reduction of 4.43%. The proposed method provides a valuable reference for fully exploiting the energy-saving potential of planetary power-split hybrid electric systems.

Keywords: planetary power-split hybrid electric vehicle; vehicle control unit; parameter calibration; sensitivity analysis; optimal Latin hypercube design; adaptive simulated annealing

Check for updates

Academic Editor: Peter Van den Bossche

Received: 8 October 2026
Revised: 14 November 2026
Accepted: 16 November 2026
Published: 18 November 2026

Copyright: © 2026 by the authors. Published by MDPI on behalf of the World Electric Vehicle Association. Licensee MDPI, Basel, Switzerland. This article is an open access article distributed under the terms and conditions of the Creative Commons Attribution (CC BY) license.

1. Introduction

Hybrid electric vehicles (HEVs) coordinate the operation of the engine and electric drive system to maintain adequate driving range while fully exploiting the advantages of the electric drive system, including high efficiency, rapid response, and regenerative braking. They have therefore become an important technological pathway for energy conservation and emission reduction in both passenger and commercial vehicles [1]. Compared with

vehicles powered by a single energy source, HEVs are characterized by the coexistence of multiple energy sources, multiple actuators, and multiple operating modes. Significant dynamic and energy coupling relationships exist among the engine, electric motors, traction battery, transmission, and clutches. As powertrain architectures become increasingly complex and operating modes more diverse, overall vehicle performance depends not only on the hardware matching of the powertrain components, but also, to a greater extent, on the coordinated management of power-source cooperation, operating-mode transitions, engine operation within high-efficiency regions, battery state-of-charge (SOC) regulation, and power-split constraints [2]. Therefore, as the core unit responsible for energy management and operational coordination in hybrid electric systems, the vehicle control unit (VCU) plays a critical role in realizing the performance potential of the powertrain and improving the overall performance of the vehicle.

Calibration of VCU control parameters is a critical step in realizing vehicle control functions and facilitating the engineering implementation of control strategies. The calibration quality directly affects vehicle dynamic response, energy utilization efficiency, driving smoothness, and operational safety [3]. In particular, parameters such as the state-of-charge (SOC) threshold, power demand threshold, charging coefficient, torque distribution coefficient, and regenerative braking intensity directly determine the power allocation among the engine, electric motors, and traction battery, thereby influencing the transition timing among operating modes such as all-electric mode, hybrid driving, and regenerative braking [4]. Therefore, without modifying the vehicle hardware architecture or the existing control strategy framework, scientific parameter optimization and calibration can further exploit the energy-saving potential of the hybrid electric system and achieve coordinated improvements in fuel economy, dynamic performance, and drivability [5]. Research on the calibration of VCU control parameters is therefore of considerable significance for enhancing the engineering applicability of control strategies, shortening the calibration cycle, and supporting energy-efficient control and intelligent calibration of hybrid electric vehicles [6].

Existing methods for the optimization and calibration of VCU control parameters can be broadly classified into two categories: engineering experience-based parameter tuning using calibration systems and systematic calibration based on optimization algorithms [7]. The former has been widely adopted in vehicle engineering development. It typically relies on commercial calibration platforms or independently developed online calibration systems to enable real-time adjustment, data acquisition, and iterative validation of parameters such as SOC thresholds, power demand thresholds, operating-mode transition boundaries, and torque distribution parameters. This approach allows parameter matching to be conducted in direct combination with test-bench experiments, hardware-in-the-loop (HIL) testing, and on-road vehicle tests, thereby offering strong engineering applicability. However, the calibration process generally relies heavily on engineers' experience and repeated trial-and-error procedures, resulting in a substantial experimental workload, prolonged development cycles, and difficulty in ensuring the global optimality of parameter combinations.

With the widespread adoption of the V-model-based modern controller development process in automotive electronics, parameter calibration has become a critical link connecting control strategy design, model-based simulation and verification, and vehicle-level implementation [8]. Internationally, the development of automotive electronic calibration tools began relatively early, resulting in a mature commercial toolchain represented by INCA from ETAS, CANape from Vector, ControlDesk/CalDesk from dSPACE, and AVL CRETA. These platforms provide comprehensive capabilities for data acquisition, online parameter adjustment, test management, and automated calibration, and have been extensively applied in vehicle and powertrain development. However, owing to the proprietary nature of commercial software and the confidentiality of the underlying technologies, their internal

parameter-optimization logic and automated calibration mechanisms are generally not fully disclosed. Moreover, most publicly available studies focus on calibration and testing of individual components or local control functions, whereas systematic optimization and calibration methods at the vehicle level under multi-parameter coupling conditions remain relatively underexplored.

In China, automotive enterprises and universities have conducted research on online calibration software for new energy vehicle controllers, CAN communication-based parameter matching platforms, and calibration verification systems for hardware-in-the-loop (HIL) testing by drawing on mature international calibration tools and development practices. Overall, domestic calibration systems have established a certain foundation for engineering applications. Nevertheless, further improvements are still required in automated optimization capability, standardization of calibration procedures, multi-parameter coupling analysis, and coordinated multi-objective optimization.

Systematic calibration methods based on design of experiments (DOE), sensitivity analysis, and intelligent optimization algorithms have been widely investigated for hybrid vehicle control parameter optimization [9–12]. Geng et al. proposed a cascaded energy management optimization method for multimode power-split hybrid electric vehicles, enabling coordinated optimization of operating-mode selection and power allocation [13]. Lin et al. developed an online-correction predictive energy management strategy integrating Q-learning-based swarm optimization with a fuzzy neural network [14]. Anselma et al. and Ferrara et al. investigated optimization-based calibration methods for hybrid and fuel-cell electric vehicles, considering energy consumption, battery thermal conditions, and component lifetime [15,16]. More directly related to VCU calibration, Du et al. applied an improved nondominated sorting genetic algorithm II (NSGA-II) to optimize operating-mode transition thresholds in rule-based control strategies for multimode hybrid electric vehicles [17]. Düzgün et al. proposed a virtual multi-objective calibration method for hybrid powertrain operating strategies and validated the controller in a hardware-in-the-loop (HIL) environment [18]. Mishra et al. and Lee et al. developed automated calibration methods for gearshift controllers based on iterative learning control and model-based optimization, respectively [19,20]. Garg et al. investigated systematic hyperparameter selection for machine-learning-based engine control to reduce calibration effort [21], while Ritzmann et al. studied the coordinated optimization of fuel consumption and NOx emissions through variable engine calibration [22]. Despite these advances, several limitations remain in existing VCU calibration studies. Many methods still rely on established calibration software and empirically defined parameter ranges, with parameters frequently refined through repeated trial-and-error procedures. Consequently, the calibration process can be time-consuming and lacks systematic theoretical guidance. In particular, systematic identification of key VCU calibration parameters and quantitative evaluation of their individual and interaction effects remain challenging for planetary power-split hybrid electric vehicles. Therefore, further research is needed to establish a systematic calibration procedure integrating parameter screening, sensitivity analysis, and optimization.

To address the aforementioned issues, this study proposes an optimization-based VCU calibration design method for a planetary power-split hybrid electric system. First, based on the architecture of the power-split hybrid electric system and a rule-based engine optimal operating strategy, the state-of-charge (SOC) threshold, power demand threshold, and charging coefficient are selected as the initial calibration parameters. Their feasible ranges are then determined by considering the battery SOC operating window, vehicle power demand, and SOC balance constraints. Second, theoretical combined fuel consumption per 100 km is adopted as the system response. Single-factor main-effect analysis is conducted to identify the influence trend of each calibration parameter, while an optimal

Latin hypercube design is employed for global sensitivity analysis to quantitatively evaluate the contributions of individual calibration parameters and their interaction terms to the fuel-consumption response. Finally, with the minimization of combined fuel consumption as the optimization objective, an adaptive simulated annealing algorithm is applied to perform global optimization of the key calibration parameters.

The main contributions of this study are summarized as follows: (1) To address the VCU parameter calibration requirements of planetary power-split hybrid electric systems, a systematic calibration framework is established, comprising calibration parameter selection, feasible-range determination, system response construction, sensitivity analysis, and optimization-based validation. This framework improves the relevance and effectiveness of control parameter selection and optimization-based calibration. (2) By integrating local sensitivity analysis with global sensitivity analysis based on an optimal Latin hypercube design, the effects of the initial calibration parameters and their interactions are quantitatively evaluated, enabling the identification of the key parameters affecting combined fuel consumption. Subsequently, with the minimization of combined fuel consumption as the optimization objective, an adaptive simulated annealing algorithm is introduced to perform global optimization of the key parameters, thereby improving the efficiency and global search capability of VCU parameter optimization and calibration.

2. Methods

2.1. Overall Design Procedure

Based on the above analysis, the overall design procedure of the proposed optimization-based VCU calibration method is illustrated in Figure 1.

First, based on the architecture and energy management strategy of the planetary power-split hybrid electric system, the power transmission relationships and operating-mode transition logic among key components, including the engine, electric motors, traction battery, planetary gear set, and clutches, are analyzed. Control parameters that exert significant effects on vehicle-level energy allocation and combined fuel consumption are then extracted as the initial calibration parameters.

Subsequently, the feasible ranges of the calibration parameters are determined by considering the battery state-of-charge (SOC) operating window, vehicle power demand distribution, operating characteristics of the engine and electric motors, and SOC balance constraints. These ranges provide the variable boundaries required for the subsequent sensitivity analysis and parameter optimization. On this basis, theoretical combined fuel consumption per 100 km is selected as the system response to characterize variations in vehicle fuel economy under different parameter combinations. During the sensitivity analysis stage, local sensitivity analysis is first performed by varying one calibration parameter at a time while keeping the remaining parameters unchanged. The resulting single-factor main-effect relationships between each calibration parameter and combined fuel consumption are used to preliminarily determine the influence trend and sensitivity level of each parameter with respect to the system response. Global sensitivity analysis is then conducted by generating sample points within the feasible parameter space through design of experiments. This analysis comprehensively considers the effects of simultaneous variations in multiple parameters and their interactions on combined fuel consumption. Statistical methods are further employed to quantitatively evaluate the contribution of each calibration parameter to the system response, thereby identifying the key calibration parameters that dominate vehicle fuel economy. Finally, with the minimization of combined fuel consumption as the optimization objective, the identified key calibration parameters are selected as the optimization variables, and an adaptive simulated annealing algorithm is employed to determine the optimized VCU parameter combination.

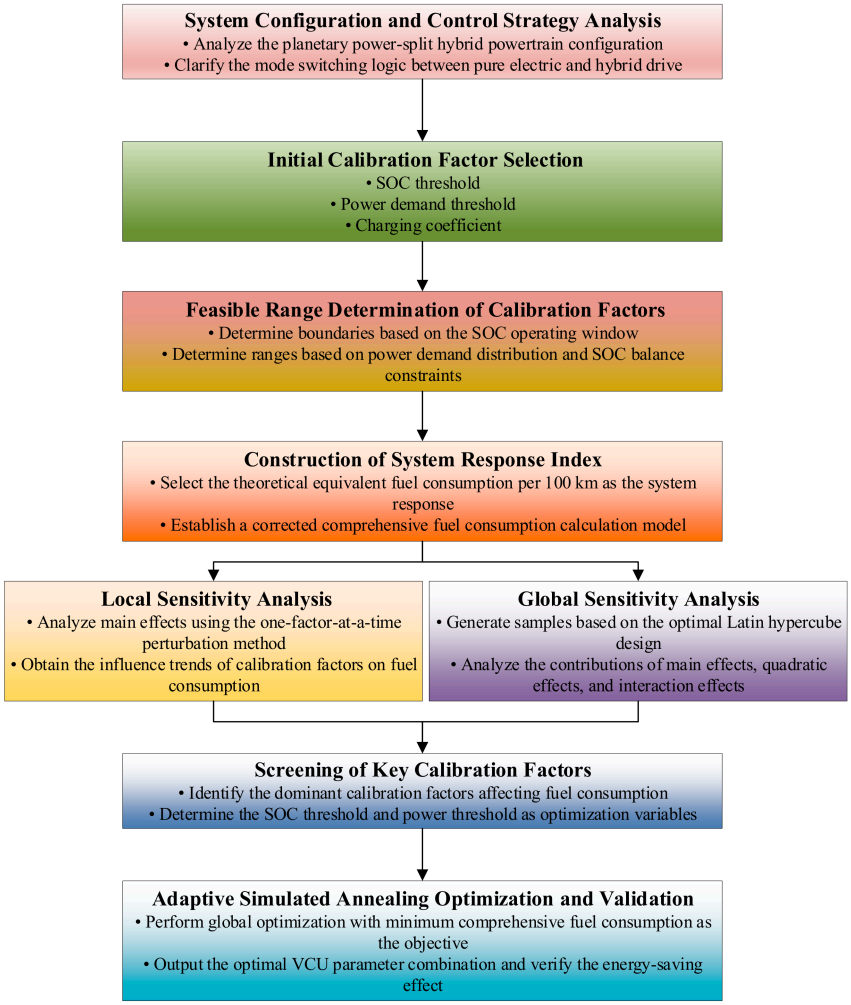


Figure 1. Overall design workflow of the calibration method.

2.2. Powertrain Architecture

The planetary power-split hybrid electric system adopted in this study is illustrated in Figure 2. This system represents a typical power-split hybrid architecture and mainly consists of a planetary gear mechanism, a traction battery, a two-speed automated manual transmission (AMT), an engine, motor MG1, motor MG2, and the clutches CL1 and CL2 for operating-mode switching. In this configuration, the engine is connected to the planetary carrier, and its power is split through the front planetary gear set: one portion is transmitted directly to the ring gear output for vehicle propulsion, while the other portion is used by motor MG1 for power generation or speed regulation. Motor MG2 is directly connected to the two-speed AMT, and its torque is combined at the ring gear output to drive the vehicle. Clutch CL1 is used to lock the planetary carrier, whereas clutch CL2 is used to lock the sun gear.

Depending on the driving requirements under different driving cycles, the powertrain can operate in four modes. The corresponding energy flow paths under these four operating modes are illustrated in Figure 3.

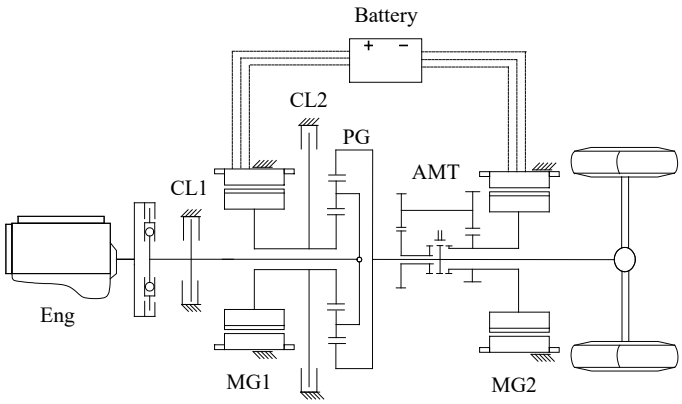


Figure 2. Schematic diagram of the powertrain configuration.

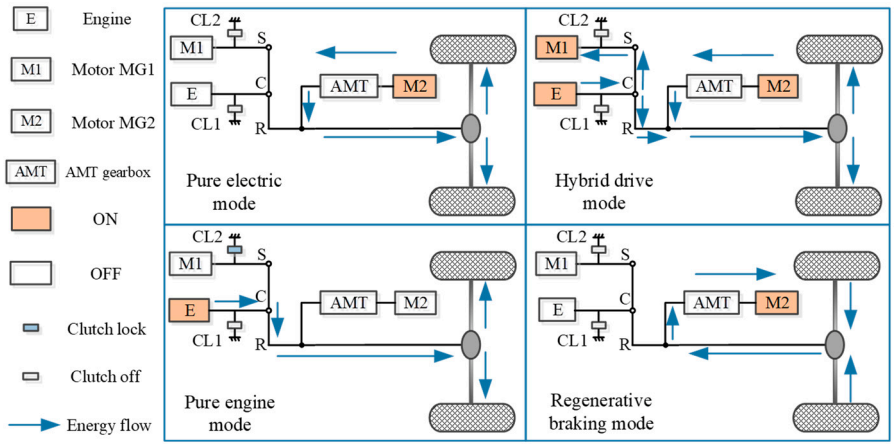


Figure 3. Energy flow diagrams of the powertrain under four operating modes.

To provide further details of the planetary gear mechanism, its geometrical parameters are summarized in Table 1.

Table 1. Geometrical parameters of the planetary gear set.

Parameter	Sun Gear	Planet Gear	Ring Gear
Number of teeth	23	19	61
Pitch diameter (mm)	96.4	79.6	255.6
Base diameter (mm)	90.4	74.7	239.7
Module (mm)		4	
Helix angle (°)		17.34	
Number of planet gears		3	
Center distance (mm)		88	

2.3. Selection of Feasible Ranges for Calibration Parameters and Response Analysis

Calibration parameters serve as the input variables for VCU parameter optimization and calibration, and their appropriate selection and feasible-range determination directly affect the subsequent sensitivity analysis and parameter optimization results. For a planetary power-split hybrid electric system, the calibration parameters should be identified according to the system architecture, operating-mode transition logic, and energy man-

agement strategy, thereby ensuring that the selected parameters adequately capture the principal characteristics of vehicle-level energy allocation and variations in fuel economy.

2.3.1. Vehicle Energy Management Strategy Analysis

In a planetary power-split hybrid electric system, the energy management strategy is primarily responsible for coordinating power allocation among the engine, electric motors, and traction battery, and for managing transitions among different operating modes according to the vehicle power demand, battery state of charge (SOC), and component operating constraints. Control parameters such as the SOC threshold, power demand threshold, and charging coefficient directly affect the engine activation timing, battery charging and discharging states, and transitions between all-electric and hybrid driving modes. Therefore, prior to the optimization and calibration of VCU parameters, the fundamental control logic of the vehicle energy management strategy should be analyzed to provide a basis for the subsequent selection of calibration parameters and determination of their feasible ranges.

The baseline control strategy adopted in this study is a rule-based engine optimal operating strategy. By defining a set of thresholds and logical rules, the strategy determines and switches the operating mode in real time according to signals such as vehicle speed, battery state of charge (SOC), and driver-requested power [23]. When the vehicle power demand is relatively low, and the battery SOC is sufficient to satisfy the propulsion requirement, the system preferentially operates in all-electric mode, in which the vehicle is driven solely by the electric motor, thereby avoiding inefficient engine operation under low-load conditions. When the power demand exceeds the specified threshold or the battery SOC approaches its control boundary, the system switches to hybrid driving mode, in which the engine and electric motor jointly provide propulsion. Under this mode, the engine is controlled to operate as far as possible within the low-fuel-consumption region of its brake-specific fuel consumption map. In this manner, the overall system efficiency can be improved while satisfying the vehicle requirements for dynamic performance and drivability [24].

From the perspective of vehicle energy management, improving fuel economy requires coordinated operation of the engine, MG1, MG2, and traction battery. Ideally, the engine should operate near its optimal fuel-efficiency region, while MG1 and MG2 should work within their respective high-efficiency regions according to the vehicle power demand and operating mode. Meanwhile, the battery should be maintained within an appropriate SOC range, with its charging and discharging power properly regulated to improve energy conversion efficiency. In the planetary power-split hybrid system investigated in this study, these components are coupled through the powertrain structure, and their operating conditions cannot be optimized independently. The VCU calibration parameters influence engine activation, operating-mode transitions, and power allocation between the engine and electric drive system, thereby affecting the overall energy utilization efficiency and combined fuel consumption.

It should be emphasized that improving engine operating efficiency is an important means of reducing fuel consumption; however, the highest engine efficiency does not necessarily correspond to the best overall fuel economy of the hybrid powertrain. Although concentrating engine operating points within a relatively narrow high-efficiency region may reduce engine-specific fuel consumption, excessive power conversion through MG1 and MG2 or unnecessary battery charging and discharging may introduce additional energy losses. Therefore, the energy management strategy should focus on optimizing the overall energy utilization efficiency of the hybrid powertrain rather than simply concentrating the engine operating points within its narrowest high-efficiency region. The optimal VCU calibration should balance engine fuel consumption, motor-generator power conversion losses, and battery charging and discharging efficiency under the required vehicle operating

conditions. Accordingly, the calibration parameters investigated in this study are intended to coordinate the operating-mode transitions and energy allocation among the powertrain components to achieve favorable overall fuel economy.

In line with the objective of VCU parameter optimization and calibration in this study, the subsequent analysis focuses on the transition between all-electric and hybrid driving modes. This transition process directly reflects the effects of the SOC threshold, power demand threshold, and their associated hysteresis-band parameters on engine activation timing and vehicle-level power allocation. The corresponding operating-mode transition conditions are presented in Table 2, and the parameters related to the control strategy are defined in Table 3.

Table 2. Operating-mode transition conditions of the control strategy.

Operating-Mode Transition	Transition Conditions
All-Electric to Hybrid Driving	$SOC \leq SOC_o \| \| P_{req} \geq P_o$
Hybrid Driving to All-Electric	$SOC \geq SOC_o + \Delta SOC_{tp}$ &&$P_{req} \leq P_o - \Delta P_{tp}$

Table 3. Definitions of key control strategy parameters.

Physical Quantity	Parameter Description
SOC (%)	Battery State of Charge
SOC_o (%)	Minimum Battery SOC Threshold
ΔSOC_{tp} (%)	SOC Threshold Hysteresis Bandwidth
P_{req} (kW)	Vehicle Power Demand
P_o (kW)	Maximum Vehicle Power Demand Threshold
ΔP_{tp} (kW)	Vehicle Power Demand Threshold Hysteresis Bandwidth

In hybrid driving mode, the engine power is required to satisfy both the vehicle propulsion power demand and the battery charging power demand:

$$P_e = P_{req} + P_{chg} = P_{req} + C_{chg} * (SOC_{thre} - SOC) \quad (1)$$

where P_{req} is the required engine power (kW); P_{chg} is the required charging power (kW); C_{chg} is the charging coefficient; and SOC_{thre} is the upper battery SOC limit for charging (%).

Meanwhile, the required engine power and battery charging power must also satisfy the physical constraints of the corresponding components:

$$P_{e,\min} \leq P_e \leq P_{e,\max} \quad (2)$$

$$0 \leq P_{chg} \leq P_{bat,ch,\max} \quad (3)$$

where $P_{e,\min}$ and $P_{e,\max}$ denote the minimum and maximum allowable engine operating powers (kW), respectively, and $P_{bat,ch,\max}$ denotes the maximum allowable charging power (kW) of the traction battery.

Furthermore, to prevent the engine operating point from exceeding its allowable operating range and to limit the adverse effects of excessive battery charging power on battery safety and service life, the required engine power and battery charging power must also satisfy the constraints expressed in Equations (2) and (3). These operating-mode transition conditions and power constraints jointly define the principal control boundaries of the rule-based energy management strategy and provide a basis for the subsequent selection of calibration parameters and determination of their feasible ranges.

According to the vehicle energy management strategy, the transition between all-electric and hybrid driving modes is primarily governed by the battery state of charge (SOC) and vehicle power demand. The SOC threshold defines the control boundary for battery participation in vehicle propulsion and SOC balance regulation. Its value directly affects the duration of all-electric operation and the variation range of the battery SOC. The power demand threshold determines the trigger condition for engine activation and therefore directly influences the transition timing between all-electric and hybrid driving modes. Consequently, the SOC threshold and power demand threshold are important control parameters affecting operating-mode transition logic and vehicle-level energy allocation, and can be selected as initial calibration parameters for VCU parameter optimization and calibration.

In hybrid driving mode, the engine output power must not only satisfy the vehicle propulsion power demand but also provide additional charging power according to the battery state of charge (SOC). The charging coefficient determines the intensity of engine-driven battery charging and consequently affects both the SOC recovery rate and the distribution of engine operating points on the brake-specific fuel consumption map. If the charging coefficient is set too low, the additional charging power supplied by the engine may be insufficient, resulting in slow SOC recovery and difficulty in maintaining SOC balance over the driving cycle. Conversely, an excessively high charging coefficient requires the engine to provide greater charging power, which may shift its operating points away from the high-efficiency region. It may also cause the SOC to rise rapidly, leading to frequent transitions between all-electric and hybrid driving modes, which is unfavorable for stable system operation and improved fuel economy. Therefore, the charging coefficient also has a significant influence on SOC balance, engine operation within the high-efficiency region, and operating-mode transition stability, and can be selected as an initial calibration parameter for subsequent sensitivity analysis and parameter optimization.

The SOC threshold should be selected to ensure that the traction battery operates within an appropriate SOC window throughout the driving cycle, thereby avoiding adverse effects on battery performance caused by overcharging or overdischarging. The power demand threshold should be determined by considering both the vehicle power demand distribution and the engine high-efficiency operating region so as to achieve a balance between vehicle dynamic performance and fuel economy. The charging coefficient should be calibrated by coordinating SOC balance, engine-driven charging intensity, and operating-mode transition stability, thereby avoiding insufficient battery charging or excessively frequent mode transitions. Accordingly, the SOC threshold, power demand threshold, and charging coefficient are selected as the initial calibration parameters in this study, and their respective value ranges are specified in Table 4. The initial values listed in the table represent the baseline calibration settings of the control strategy and serve as references for the subsequent local sensitivity analysis, global sensitivity analysis, and parameter optimization.

Table 4. Feasible ranges of the calibration parameters.

Calibration Parameter (Unit)	Feasible Range	Initial Value
SOC_o (%)	[40,85]	72
C_{chg}	[10,40]	20
P_o (kW)	[6,37]	27

2.3.2. System Response

The SOC threshold, power demand threshold, and charging coefficient selected in this study primarily affect the transition boundaries between all-electric and hybrid driv-

ing modes, as well as the adjustment of engine operating points under hybrid driving conditions. Their effects are therefore mainly reflected in vehicle-level energy allocation and fuel economy. Since these parameters do not alter the specifications of the powertrain components, the driveline architecture, or the maximum power output capability, their influence on boundary indicators of dynamic performance, such as maximum vehicle speed, acceleration capability, and gradeability, is relatively limited. In accordance with the objective of this study, the subsequent calibration response analysis focuses on vehicle fuel economy. Theoretical combined fuel consumption per 100 km is selected as the system response to characterize variations in vehicle-level energy utilization efficiency under different parameter combinations.

Based on energy consumption analysis, a method for calculating the combined fuel consumption is established, yielding the following unified theoretical model for the SOC-corrected combined fuel consumption of the hybrid electric system.

First, considering the energy conversion efficiencies of the relevant components, calculate the effective energy that can be retransmitted to the wheels after regenerative braking recovery:

$$E_{reg} = E_{rgb}\eta_{tr,c}\eta_{b,c}\eta_{b,dc} \tag{4}$$

where E_{rgb} represents the regenerative braking energy recovered at the battery end (kJ), and $\eta_{tr,c}$,$\eta_{b,c}$, and $\eta_{b,dc}$ represent the energy conversion efficiency coefficients of the respective stages.

Therefore, after deducting the recovered regenerative braking energy, the remaining required energy at the wheels can be expressed as

$$E_{rem} = E_{wh} - E_{reg} \tag{5}$$

Substituting the expression for effective regenerative braking energy into the above equation yields

$$E_{rem} = E_{wh}[1 - \frac{E_{rgb}}{E_{wh}}\eta_{tr,c}\eta_{b,c}\eta_{b,dc}] \tag{6}$$

Further considering the average efficiency of the transmission system η_{tr}, the corresponding output energy of the engine can be obtained:

$$E_e = \frac{E_{rem}}{\eta_{tr}} \tag{7}$$

Finally, combining the average fuel consumption rate of the engine $b_{e,avg}$ (g/kWh) and the fuel-to-electricity conversion coefficient C the SOC-corrected comprehensive fuel consumption can be calculated as

$$f_{e,u} = E_{wh} \cdot \left[1 - \frac{E_{rgb}}{E_{wh}}\eta_{tr}\eta_{b,c}\eta_{b,dc}\right] \cdot \frac{b_{e,avg} \cdot C}{\eta_{tr}} \tag{8}$$

where $f_{e,u}$ represents the SOC-corrected comprehensive fuel consumption (L/100 km), E_{wh} represents the total required energy at the wheels (kJ). The fuel-to-electricity conversion coefficient C is set to 0.245 in this study [25]. This coefficient is derived based on the equivalent energy method, considering the average energy conversion efficiency of the motor/generators and the fuel thermal value.

This formula establishes the relationship between wheel energy demand, regenerative braking energy recovery, powertrain energy conversion efficiency, and fuel consumption, providing a unified basis for evaluating comprehensive fuel consumption under different VCU calibration parameter configurations.

To account for the SOC difference between the beginning and the end of each driving cycle, an energy-based correction is introduced in the combined fuel consumption calculation. The battery energy variation is calculated as

$$\Delta E_{SOC} = E_{bat,nom}(SOC_{ini} - SOC_{end}) \tag{9}$$

where $E_{bat,nom}$ denotes the nominal battery energy capacity, and SOC_{ini} and SOC_{end} represent the initial and final battery SOC, respectively. A positive value of ΔSOC indicates net battery energy depletion, whereas a negative value indicates an increase in stored battery energy. The corresponding energy difference is considered in the overall energy balance and converted into equivalent fuel consumption using the energy conversion coefficients in Equation (8). This correction accounts for variations in battery energy over the driving cycle and ensures a more consistent comparison of fuel consumption among different VCU calibration strategies. The theoretical fuel consumption model adopted in this study is based on the energy-flow analysis framework established in our previous work [26]. In that study, the unified fuel economy model was evaluated by comparing theoretical calculations with vehicle test results for different hybrid electric powertrain configurations, including a planetary power-split system. This previous investigation provides a methodological basis for the SOC-corrected theoretical fuel consumption evaluation employed in the present study.

2.4. Sensitivity Analysis of Calibration Parameters

The VCU calibration process essentially involves adjusting the calibration parameters and applying sensitivity analysis to identify the intrinsic relationships between the calibration parameters and the calibration response, thereby determining the relative importance of each calibration parameter to the system response [27]. Commonly used sensitivity analysis methods can be classified into local sensitivity analysis and global sensitivity analysis [28,29].

2.4.1. Local Sensitivity Analysis

After defining the system response, a local sensitivity analysis is first conducted using the one-factor-at-a-time perturbation method to preliminarily identify the independent effects of individual calibration parameters on vehicle fuel economy. The calibration parameter vector is defined as

$$X = [x_1, x_2, \cdots, x_n]^T \tag{10}$$

where x_1, x_2, and x_3 denote the SOC threshold, power demand threshold, and charging coefficient, respectively. The system response is denoted by

$$y = f(x) \tag{11}$$

where y denotes the theoretical combined fuel consumption (L/100 km), and $f(x)$ represents the parameter–response mapping established by the vehicle control strategy model and the fuel consumption calculation model.

During the local sensitivity analysis, only one target calibration parameter, x_i, is varied at a time, while the remaining calibration parameters are maintained at their initial values. The target parameter is sampled at equally spaced intervals within its feasible range, $[x_i^L, x_i^U]$, as follows:

$$x_i^{(k)} = x_i^L + \frac{k-1}{m-1}(x_i^U - x_i^L), k = 1, 2, \ldots, m \tag{12}$$

where x_i^L and x_i^U denote the lower and upper bounds of the ith calibration parameter, respectively, and m is the number of sampling points for this parameter within its feasible range. The corresponding system response can be expressed as

$$y_i^{(k)} = f(x_{1,0}, \cdots, x_{i-1,0}, x_i^{(k)}, x_{i+1,0}, \cdots, x_{n,0}) \tag{13}$$

where $x_{j,0}$ denotes the initial value of the jth calibration parameter.

During the local sensitivity analysis, the single-factor main-effect relationship between the ith calibration parameter and the system response can be obtained by varying this parameter while holding all other calibration parameters constant:

$$y_i = g_i(x_i) \tag{14}$$

$$g_i(x_i) = f(x_{1,0}, \ldots, x_{i-1,0}, x_i, x_{i+1,0} \ldots, x_{n,0}) \tag{15}$$

where $g_i(x_i)$ denotes the single-factor response function corresponding to the ith calibration parameter. As x_i varies within its feasible range, the corresponding system responses y_i form the single-factor main-effect curve of that calibration parameter. This curve characterizes the influence trend of the target calibration parameter (L/100 km).

To further quantify the local influence of different calibration parameters, a normalized local sensitivity coefficient is defined as follows:

$$S_i^{loc} = \frac{\max(y_i) - \min(y_i)}{y_0} \cdot \frac{x_{i,0}}{x_i^U - x_i^L} \tag{16}$$

where y_0 denotes the theoretical combined fuel consumption per 100 km under the initial calibration parameter combination; $\max(y_i)$ and $\min(y_i)$ denote the maximum and minimum system responses, respectively, obtained while varying the ith calibration parameter. A larger S_i^{loc} indicates that the calibration parameter has a more significant influence on the system response within the local range, whereas a smaller (S_i) indicates weaker local sensitivity of the combined fuel consumption to that parameter.

2.4.2. Global Sensitivity Analysis

Local sensitivity analysis can reveal the independent influence of an individual calibration parameter. However, its results depend on the fixed values assigned to the remaining parameters and therefore cannot adequately capture the effects of simultaneous variations in multiple calibration parameters or the interactions among them on the system response [30]. Accordingly, this study further employs a design-of-experiments-based global sensitivity analysis method to quantitatively evaluate the combined effects of the calibration parameters over the entire feasible parameter space.

Let the experimental sample matrix used for the global sensitivity analysis be defined as

$$X = \begin{bmatrix} x_1^{(1)} & x_2^{(1)} & \ldots & x_n^{(1)} \\ x_1^{(2)} & x_2^{(2)} & \ldots & x_n^{(2)} \\ \vdots & \vdots & \ddots & \vdots \\ x_1^{(N)} & x_2^{(N)} & \ldots & x_n^{(N)} \end{bmatrix} \tag{17}$$

where N denotes the number of design-of-experiments samples, with $N = 200$ in this study, and n denotes the number of calibration parameters, with $n = 3$. Each sample satisfies the following constraint:

$$x_i^L \le x_i^{(r)} \le x_i^U, r = 1, 2, \cdots, N \tag{18}$$

To eliminate the effects of differences in units and value ranges among the calibration parameters on the statistical analysis, each calibration parameter is normalized as follows:

$$z_i^{(r)} = \frac{x_i^{(r)} - x_i^L}{x_i^U - x_i^L} \tag{19}$$

where $z_i^{(r)}$ denotes the normalized value of the ith calibration parameter in the rth sample. By inputting each sample into the vehicle control strategy model, the corresponding sequence of system responses can be obtained as

$$Y = \left[y^{(1)}, y^{(2)}, \cdots, y^{(N)}\right]^T \tag{20}$$

To quantitatively characterize the effects of individual calibration parameters and their interaction terms on the system response, a quadratic response surface model is employed to fit the sample data:

$$\hat{y} = \beta_0 + \sum_{i=1}^{n} \beta_i z_i + \sum_{i=1}^{n} \beta_{ii} z_i^2 + \sum_{i=1}^{n-1} \sum_{j=i+1}^{n} \beta_{ij} z_i z_j \tag{21}$$

where $\hat{y}$ denotes the fitted theoretical combined fuel consumption (L/100 km); β_0 is the constant term; β_i denotes the main-effect coefficient of the ith calibration parameter; β_{ii} denotes the quadratic-effect coefficient of the ith calibration parameter; and β_{ij} denotes the interaction-effect coefficient between the ith and jth calibration parameters. A larger absolute coefficient indicates a stronger influence of the corresponding parameter or interaction term on the system response.

To further construct the Pareto chart, the effect coefficients of the individual terms can be converted into contribution ratios as follows:

$$C_q = \frac{\left|\beta_q\right|}{\sum_{q=1}^{M} \left|\beta_q\right|} \times 100\% \tag{22}$$

where C_q denotes the relative coefficient-based effect index of the q-th model term, β_q represents its regression coefficient, and M is the total number of terms included in the response surface model. Since all calibration parameters are normalized before regression, the coefficient magnitudes can be compared within the constructed response surface model. The resulting index is used to provide a relative ranking of the fitted main, quadratic, and interaction effects. It should be noted that this coefficient-based index represents the relative magnitude of regression coefficients rather than a formal decomposition of the response variance. Therefore, it is used as a preliminary screening indicator to identify potentially influential calibration parameters, rather than as a variance-based sensitivity measure.

Design of experiments (DOE) can effectively characterize the features of the parameter space using a limited number of samples, thereby reducing the experimental and computational costs required for global sensitivity analysis. In this study, calibration parameter samples are generated using the DOE method, and the resulting system responses are analyzed to investigate the effects of individual parameters and their interaction terms. The implementation procedure is described below.

As shown in Figure 4, the DOE procedure mainly consists of four steps: system response determination, selection of experimental design factors, selection of the DOE method, and analysis of the results. First, the theoretical combined fuel consumption per 100 km is selected as the system response. Second, the calibration parameters are selected as the experimental design variables. Third, an optimal Latin hypercube design (Opt LHD) is employed to generate the sample points. Finally, the main effects and interaction effects of the calibration parameters are analyzed based on the corresponding sample responses, thereby identifying the key calibration parameters that have significant effects on the system response.

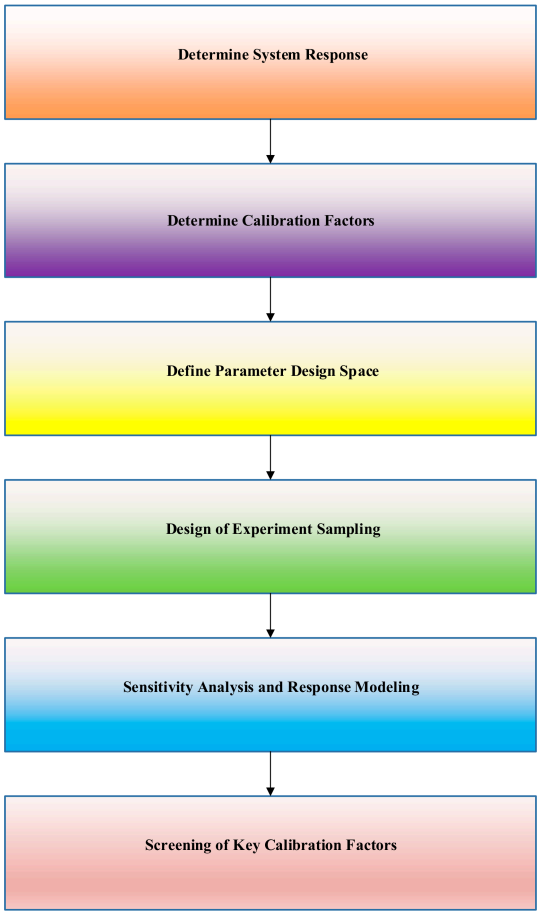


Figure 4. Process of design of experiments and sensitivity analysis.

2.5. Optimization of Key Calibration Parameters

Following the selection of the calibration parameters and the establishment of the sensitivity analysis framework, this study further optimizes the key parameters that affect the operating-mode transition boundaries and vehicle-level power allocation. Since the SOC threshold and power demand threshold define the battery SOC control boundary and the engine activation power boundary, respectively, both parameters directly influence transitions between all-electric and hybrid driving modes. They are therefore selected as the optimization variables, and an optimization model for the key calibration parameters is formulated with the objective of minimizing the theoretical combined fuel consumption per 100 km:

$$\min_{x} f(x) = f_{eu}(x) \tag{23}$$

$$x = [SOC_o, P_o]^T, SOC_o^L \le SOC_o \le SOC_o^U, P_o^L \le P_o \le P_o^U \tag{24}$$

where x denotes the vector of key calibration parameters, and $f(x)$ is the objective function, representing the theoretical combined fuel consumption (L/100 km) under different calibration parameter combinations. SOC_o^L and SOC_o^U denote the lower and upper bounds of the feasible range of the SOC threshold (%), respectively, while P_o^L and P_o^U denote the lower and upper bounds of the feasible range of the power demand threshold (kW), respectively.

Considering the nonlinear mapping between the VCU control parameters and combined fuel consumption, as well as the possible presence of multiple local optima in the optimization process, a global search algorithm is employed to optimize the key calibration parameters. Among the available methods, the adaptive simulated annealing algorithm imposes relatively few requirements on the continuity and differentiability of the objective function and exhibits strong global search capability and robustness. It is therefore

well suited to nonconvex and nonlinear optimization problems involving strong parameter coupling. Inspired by the thermodynamic annealing process, the algorithm starts from a randomly generated initial solution and continuously perturbs the current solution to generate candidate solutions. Whether a candidate solution is accepted is determined according to the resulting change in the objective function. Let the current solution be x_k, and let the perturbed candidate solution be x_{new}. The change in the objective function is then expressed as

$$\Delta f = f(x_{new}) - f(x_k) \tag{25}$$

When $\Delta f < 0$, the candidate solution reduces the combined fuel consumption and is therefore accepted directly. When $\Delta f > 0$, the candidate solution is inferior to the current solution and is accepted with a certain probability according to the Metropolis criterion. The corresponding acceptance probability is given by

$$P_{accept} = \exp(-\frac{\Delta f}{T_k}) \tag{26}$$

where T_k denotes the annealing temperature at the kth iteration. This acceptance criterion enables the algorithm to accept inferior solutions with a relatively high probability during the early stages of the search, thereby escaping local optima and expanding the search space.

As the temperature gradually decreases, the probability of accepting inferior solutions is reduced, and the algorithm progressively shifts toward a refined local search, ultimately converging to the optimal region. Compared with the conventional simulated annealing algorithm, the adaptive simulated annealing algorithm dynamically adjusts the search step size and annealing schedule, thereby achieving an improved balance between convergence speed and solution accuracy. Therefore, the adaptive simulated annealing algorithm is employed in this study to perform global optimization of the key calibration parameters, and the corresponding algorithmic procedure is illustrated in Figure 5.

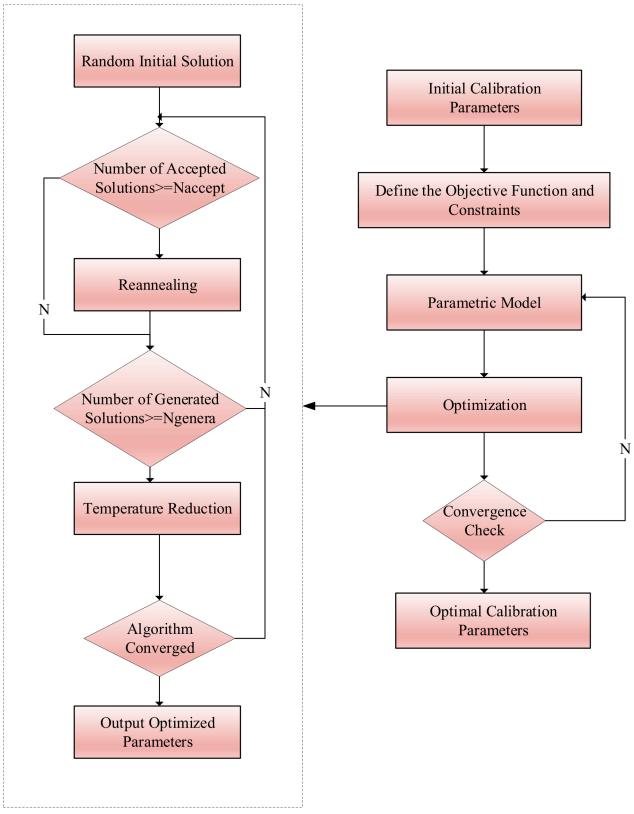


Figure 5. Flowchart of the adaptive simulated annealing algorithm.

3. Results

In this section, the proposed optimization-based VCU calibration method is applied to a planetary power-split hybrid electric bus, and its validity and effectiveness are verified through detailed analysis of the simulation results. The basic parameters of the planetary power-split hybrid electric bus are listed in Table 5, while the parameters of its key components are provided in Table 6.

Table 5. Basic vehicle parameters.

Parameter	Value
Gross Vehicle Mass/kg	16,320
Curb Mass/kg	10,030
Aerodynamic Drag Coefficient	0.58
Frontal Area/m^2	7.81
Wheel Rolling Radius/m	0.518
Rolling Resistance Coefficient	0.0072

Table 6. Key component parameters.

Parameter		Value
Engine	Peak torque/Nm	810
	Maximum power/kW	150
Motor MG1	Peak power/kW	120
	Rated power/kW	80
	Maximum speed/(r/min)	5000
	Peak torque/Nm	250
Motor MG2	Peak power/kW	130
	Rated power/kW	83
	Maximum speed/(r/min)	5800
	Peak torque/Nm	550
Planetary gear set	Characteristic parameter	2.5
Two-speed AMT	First-gear ratio	7
	Second-gear ratio	2.5
Traction battery	Voltage/V	600
	Maximum power/kW	90
	Total energy/kWh	30
	Capacity/Ah	50

Based on the above analysis, the adaptive simulated annealing algorithm was implemented in MATLAB 2023b (The MathWorks, Inc., Natick, MA, USA) to optimize the two key calibration parameters, namely, the power demand threshold and the SOC threshold. The maximum number of iterations was set to 1000, and convergence was evaluated every five iterations using a tolerance of 1.0×10^{-8}. To account for constraint violations during the optimization process, a penalty function with a scaling factor of 1000 and an exponent

of 2 was employed. These settings were used in the subsequent parameter optimization and convergence analysis.

The parameters listed in Tables 5 and 6 provide the basis for vehicle energy consumption analysis and VCU calibration optimization. Specifically, the vehicle mass, aerodynamic drag coefficient, frontal area, and rolling resistance coefficient in Table 5 determine the vehicle driving resistance and power demand, thereby affecting fuel consumption. The engine, MG1, MG2, and battery parameters in Table 6 define the power capabilities and operating constraints of the hybrid powertrain, while the planetary gear set and transmission ratios determine the power transmission characteristics. These parameters collectively establish the vehicle operating conditions for subsequent simulation analyses. Based on this vehicle configuration, the present study focuses on optimizing VCU calibration parameters to improve operating-mode transitions, energy allocation, and fuel economy.

The Chinese City Bus Cycle (CCBC) was adopted to evaluate the proposed VCU calibration method under representative urban bus operating conditions. The corresponding speed–time profile is shown in Figure 6, covering typical acceleration, deceleration, low-speed driving, and frequent stop-and-go conditions. The same driving cycle and vehicle parameters were used for the sensitivity analysis and parameter optimization to ensure a consistent comparison of theoretical combined fuel consumption under different calibration settings.

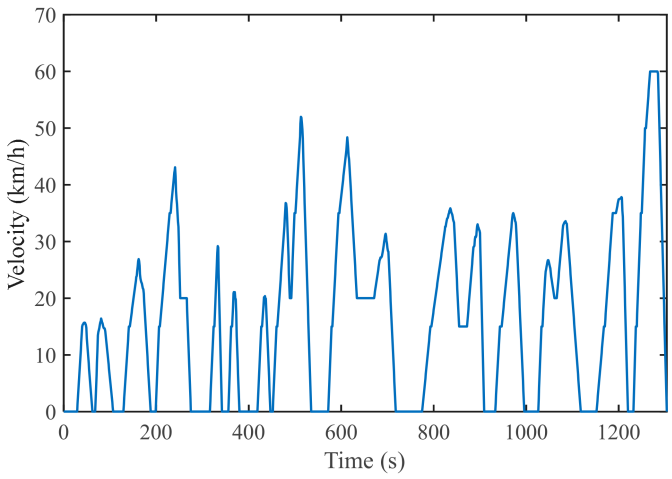
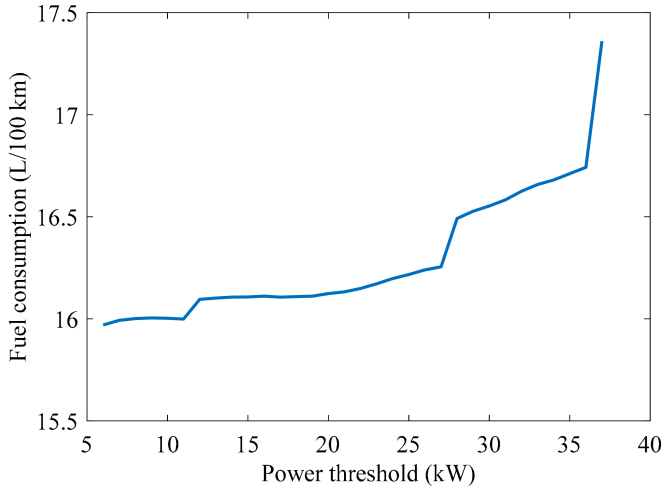


Figure 6. CCBC.

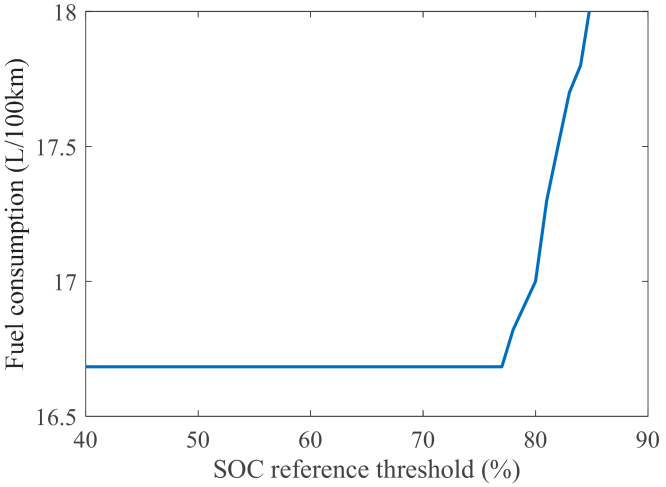
3.1. Results of Local Sensitivity Analysis

By sequentially varying the power demand threshold, SOC threshold, and charging coefficient within their respective feasible ranges and taking the theoretical combined fuel consumption per 100 km as the dependent variable, the single-factor main-effect plots shown in Figure 7 were obtained. These plots provide an intuitive representation of the parameter–response mapping relationships.

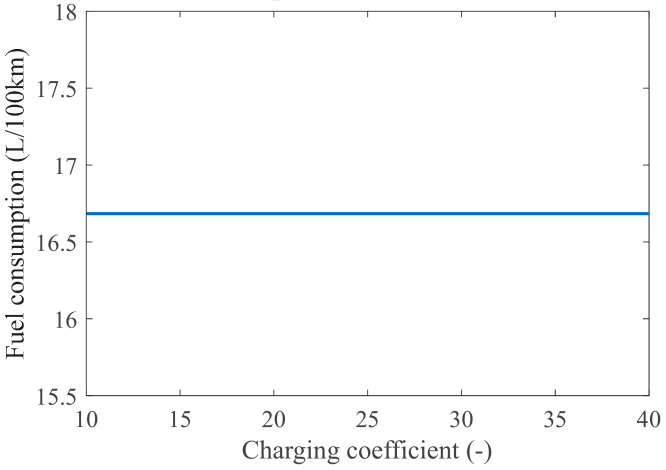
The curves presented in Figure 7 illustrate how variations in VCU calibration parameters affect the predicted combined fuel consumption through changes in operating-mode transitions and vehicle-level energy allocation.



(**a**) Main-effect plot of the power demand threshold



(**b**) Main-effect plot of the SOC threshold



(**c**) Main-effect plot of the charging coefficient

Figure 7. Main-effect plots of the calibration parameters.

(1) The combined fuel consumption increases monotonically with the power demand threshold. A lower power demand threshold advances engine activation, thereby narrowing the power range of all-electric operation and increasing hybrid-mode participation. Under the rule-based engine optimal operating strategy, earlier engine engagement improves the coordination between engine operation and battery power utilization, resulting in lower combined fuel consumption.

(2) The effect of the SOC threshold on combined fuel consumption exhibits a distinct characteristic under the initial calibration parameter combination. When the SOC threshold is below approximately 78%, variations in this parameter have almost no effect on fuel consumption. This is because the initial battery SOC was set to 80%, while the minimum SOC recorded during this specific simulation was approximately 78%. Therefore, the SOC threshold did not become an active control boundary within this range. It should be noted that this result represents the local sensitivity analysis under the initial parameter settings, rather than a fixed SOC trajectory applicable to all calibration parameter combinations.

(3) Within the feasible range of the charging coefficient, no significant variation in combined fuel consumption is observed. This is mainly because the SOC threshold remains at its initial value of 72% during the local sensitivity analysis, while the battery SOC stays above this threshold throughout the simulation. Consequently, the engine-driven battery charging regulation is not effectively activated. Although the charging coefficient varies, it produces limited changes in engine-driven charging power and engine operating-point distribution, resulting in a relatively small influence on combined fuel consumption.

Overall, variations in the three VCU calibration parameters affect the predicted fuel consumption by modifying engine activation timing, battery energy utilization, and engine-driven charging power. These changes alter the vehicle-level energy allocation and are ultimately reflected in the SOC-corrected combined fuel consumption calculated using Equation (8).

The local sensitivity analysis results indicate that the power demand threshold P_o exerts the most significant influence on combined fuel consumption over its entire feasible range and exhibits a positive correlation with the system response. The effect of the SOC_o threshold on combined fuel consumption is clearly range-dependent, becoming pronounced only when the threshold exceeds 78%. Under the initial calibration parameter combination, the charging coefficient has a relatively limited effect on the fuel-consumption response, whereas the SOC threshold and power demand threshold exhibit higher sensitivities to variations in combined fuel consumption. These results provide a preliminary basis for identifying the key calibration parameters. Accordingly, global sensitivity analysis is required to further improve the reliability of key calibration parameter identification.

3.2. Results of Global Sensitivity Analysis

An optimal Latin hypercube design was employed to sample the feasible parameter space, and a total of 200 DOE samples were generated for the analysis. The distribution of the sample points in the three-dimensional parameter space is shown in Figure 8. To clearly present the distribution characteristics of all calibration parameters in a single Figure, each parameter was normalized. The 200 sample points generated using the optimal Latin hypercube design are uniformly distributed throughout the feasible parameter space, providing comprehensive coverage of the entire design domain.

The 200 sample sets were used as input variables and sequentially fed into the vehicle control strategy model. Simulations were then performed to obtain the theoretical combined fuel consumption per 100 km corresponding to each calibration parameter combination, as shown in Figure 9. As shown in Figure 9, the 200 DOE simulations exhibit noticeable variations in theoretical combined fuel consumption under different parameter combinations, indicating that the selected calibration parameters jointly affect vehicle energy utilization. The calculated fuel consumption responses are distributed over a relatively broad range, and the preliminary minimum value is approximately 16.0 L/100 km. This variation confirms that the selected parameter space adequately captures different fuel economy responses and provides a basis for constructing the quadratic response surface model.

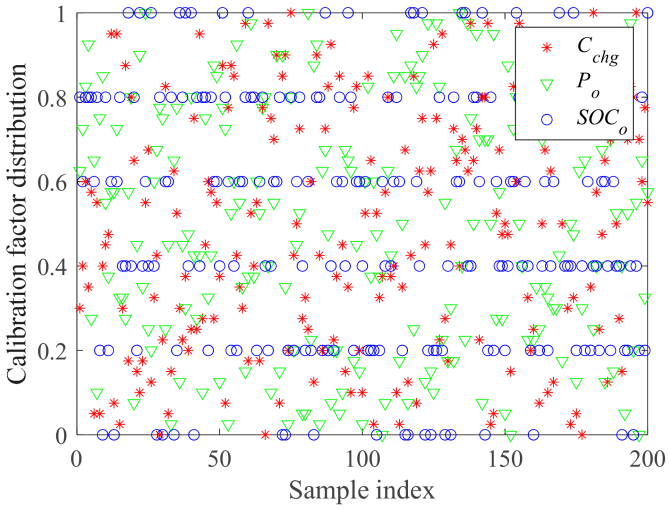


Figure 8. Sample-space distribution of 200 calibration-parameter sets.

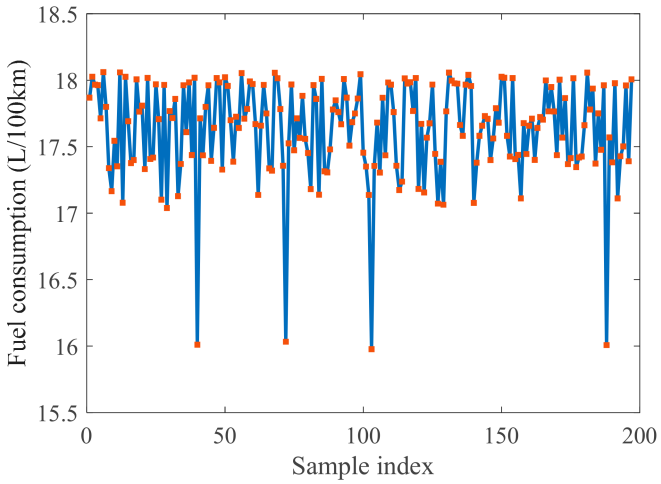


Figure 9. Simulation results of combined fuel consumption.

To further examine the relative effects of the calibration parameters and their interactions on the system response, the coefficient-based effect indices obtained from the quadratic response surface model were used to construct a Pareto chart, as shown in Figure 10. The bars represent the relative magnitudes of the fitted regression coefficients, with positive and negative signs indicating the directions of the corresponding effects. Larger absolute indices indicate relatively stronger fitted effects within the response surface model. These results provide a preliminary ranking of the calibration parameters and their interaction terms for subsequent parameter screening.

As shown in Figure 10, the power demand threshold and SOC threshold exhibit relatively larger coefficient-based effect indices than the charging coefficient. Their fitted main effects are therefore identified as the dominant terms in the response surface model. Although the charging coefficient and some interaction terms also influence the response, their relative coefficient magnitudes are comparatively smaller. Based on this preliminary effect ranking, the power demand threshold and SOC threshold are selected as the primary calibration parameters for subsequent optimization. This screening result is interpreted in terms of the relative magnitudes of the fitted model coefficients rather than the percentage contributions to the total response variance.

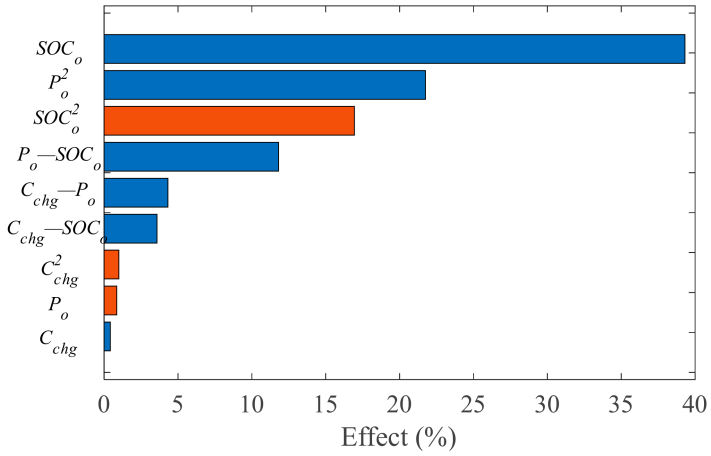


Figure 10. Relative coefficient-based effect indices of calibration parameters.

3.3. Results of Optimization of Key Calibration Parameters

Through global sensitivity analysis, the power demand threshold P_o and SOC_o threshold have been identified as the key calibration parameters affecting the vehicle's combined fuel consumption. To further exploit the energy-saving potential of the system and reduce combined fuel consumption, an appropriate numerical optimization method is required to determine the optimal values of these two key parameters.

To address the strong parameter coupling, pronounced nonlinearity of the fuel-consumption response, and susceptibility to local optima in VCU calibration, an adaptive simulated annealing (ASA) algorithm is introduced to perform global optimization after screening the key calibration parameters. The ASA algorithm was selected because its probabilistic acceptance mechanism and adaptive search strategy are suitable for nonlinear VCU parameter optimization involving coupled calibration variables. Specifically, the Metropolis criterion allows occasional acceptance of inferior solutions, providing a mechanism for escaping local optima, while the adaptive annealing schedule and dynamic search step size facilitate the adjustment of global exploration and local refinement during optimization. Following sensitivity-based parameter screening, ASA is applied to the reduced-dimensional calibration problem to identify a favorable parameter combination. This optimization procedure is integrated with the preceding sensitivity analysis, thereby improving the reliability of the VCU parameter calibration results while reducing the number of optimization variables.

The optimization trajectory of the vehicle's combined fuel consumption is shown in Figure 11. The dynamic evolution of the optimization process can be clearly observed. During the initial stage, the algorithm starts from the initial solution, and the objective function exhibits relatively large fluctuations. This indicates that the adaptive simulated annealing algorithm possesses strong stochastic search capability at high annealing temperatures, enabling extensive exploration of the design space. As the annealing temperature gradually decreases, the probability of accepting inferior solutions is progressively reduced. Although occasional fluctuations remain in the optimization trajectory, the objective function exhibits a clear overall downward trend. This process demonstrates the dual advantages of the adaptive simulated annealing algorithm. On the one hand, the probabilistic acceptance mechanism enables the algorithm to escape the current local optimum and effectively avoids premature convergence to local optima. On the other hand, the gradual convergence of the search process allows the algorithm to ultimately identify the region containing the global optimum.

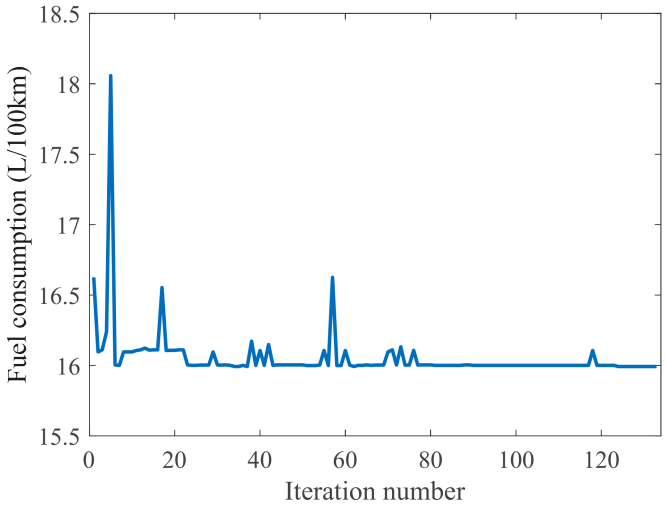


Figure 11. Iterative optimization process of key calibration parameters.

The optimization trajectory shown in Figure 11 demonstrates the convergence behavior of the adaptive simulated annealing algorithm. During the initial search stage, the objective function exhibits relatively large fluctuations, reflecting the extensive exploration of the parameter space. As the optimization proceeds, the overall fuel-consumption response gradually decreases despite occasional fluctuations caused by the probabilistic acceptance of candidate solutions. After approximately the 133rd iteration, the objective function becomes stable, and no further significant improvement is observed. This indicates that the algorithm has identified a stable optimal parameter region within the prescribed search range.

As indicated by the optimization iterations, the objective function value becomes stable after the 133rd iteration, and no further significant variation is observed in the vehicle's combined fuel consumption, indicating that the optimization process has converged. This result demonstrates that the adaptive simulated annealing algorithm can effectively search for the key calibration parameters within a limited number of iterations and obtain stable parameter optimization results.

Through global optimization of the power demand threshold P_o and SOC threshold using the adaptive simulated annealing algorithm, the optimal combination of the key calibration parameters was ultimately obtained.

As summarized in Table 7, after optimization, the SOC threshold decreased from 72% to 55%, whereas the power demand threshold decreased from 27 kW to 7 kW. It is important to distinguish this joint optimization result from the preceding local sensitivity analysis, in which only one parameter was varied while the remaining parameters were maintained at their initial values. During the joint optimization process, simultaneous changes in the SOC threshold and power demand threshold modify the operating-mode transition boundaries and power allocation conditions, and may consequently alter the battery SOC trajectory. Therefore, the minimum SOC of approximately 78% observed in the initial simulation should not be directly applied to the optimized parameter combination. The reduction in theoretical combined fuel consumption from 16.71 L/100 km to 15.97 L/100 km represents the overall effect of the optimized parameter combination, rather than the isolated contribution of the SOC threshold adjustment.

Table 7. Comparison of calibration parameters before and after optimization.

Calibration Parameter (Unit)	Before Optimization	After Optimization
SOC_o (%)	72	55
P_o (kW)	27	7
$f_{e,u}$ (L/100 km)	16.71	15.97

It should be noted that the use of fixed calibration thresholds does not imply that the control strategy relies on a single parameter to determine vehicle operating modes. In practical VCU development, threshold-based rule control is widely adopted because of its clear control logic, limited computational requirements, and convenient calibration and implementation. In the present study, the SOC threshold and power demand threshold jointly determine the operating-mode transition conditions, while the charging coefficient regulates engine-driven battery charging behavior. These parameters perform different but complementary functions in the energy management strategy. Based on practical powertrain development and calibration experience, this threshold-based approach provides a reasonable balance between control effectiveness and engineering implementability. Therefore, the objective of this study is not to replace the existing rule-based control structure with a more complex adaptive strategy, but to systematically identify and optimize its key calibration parameters to improve fuel economy.

To rigorously address the potential logical circularity regarding the screening of the charging coefficient, a post-optimization sensitivity analysis was conducted. Although the initial local sensitivity analysis was performed at $SOC_o = 72\%$ where C_{chg} was inactive, the optimized SOC threshold is reduced to 55%, which may activate the engine-driven charging boundary. To evaluate this, the optimized parameters were fixed, and a single-factor perturbation was performed across its feasible range ([10,40]).

As shown in Figure 12, the combined fuel consumption fluctuates marginally between 15.97 L/100 km and 16.05 L/100 km, with a maximum discrepancy of less than 0.5%. This demonstrates that C_{chg} remains a secondary parameter even under the optimized lower-SOC operational window. The physical mechanism is twofold: First, the optimized power demand threshold is significantly reduced to 7 kW, enabling earlier engine activation. The baseline engine generation during the CCBC is thus sufficient to maintain SOC balance, minimizing reliance on active charging regulation. Second, under the low-speed, frequent stop-and-go CCBC, the SOC deviation term remains relatively small; consequently, the calculated charging power is constrained by the engine's optimal operating line and the battery's charging power limit, effectively diminishing the regulatory effect of C_{chg}. Therefore, excluding C_{chg} from the final optimization is justified, as it reduces computational dimensions without compromising the validity of the final parameter set.

To verify whether the boundary solution of 7 kW is constrained by the lower search bound, and to validate the physical constraints of the single-objective optimization, a range sensitivity analysis and constraint verification were conducted. The lower bound of P_o was extended from 6 kW to 0 kW, and the resulting variations in combined fuel consumption and engine start-stop frequency are illustrated in Figure 13.

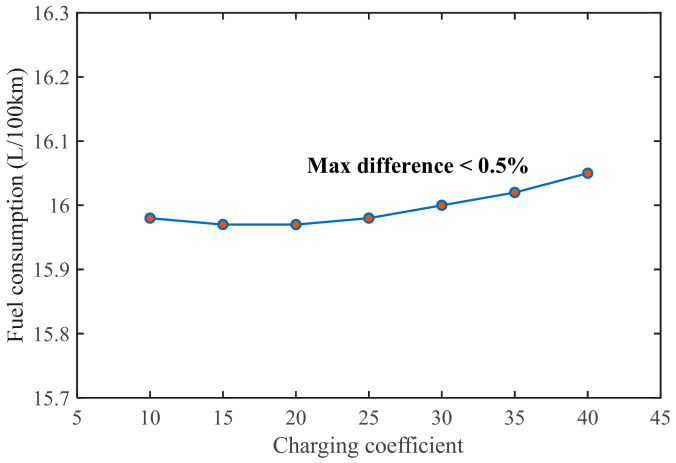


Figure 12. Post-optimization sensitivity analysis of the charging coefficient.

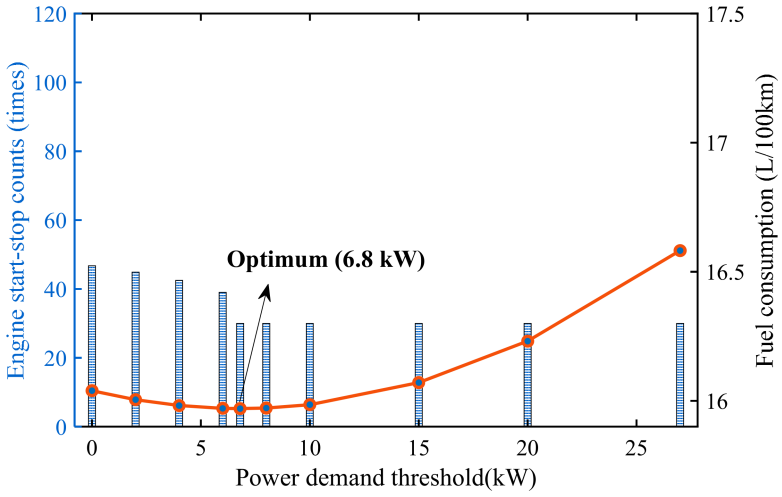


Figure 13. Range sensitivity analysis of the power demand threshold.

The re-optimization results indicate that the true optimum converges to approximately 6.8 kW. When P_o drops below this threshold, the engine is forced to start in extremely low-load regions. This leads to a rapid deterioration of brake-specific fuel consumption (BSFC), which offsets the electric driving benefits and causes the fuel consumption curve to rebound. Furthermore, as shown by the left Y-axis in Figure 13, excessively low P_o values trigger a sharp increase in engine start-stop frequency, which is detrimental to NVH and drivability.

Therefore, the obtained 7 kW represents a favorable fuel-economy-oriented calibration result rather than an artificial boundary artifact under the investigated conditions. The supplementary evaluation also indicates that the SOC deviation decreased from 21% to 12%, while the engine start-stop frequency at 7 kW remained within a relatively moderate range compared with those observed at excessively low power demand thresholds. It is worth emphasizing that although the objective function primarily targets fuel consumption, the additional assessment of engine start-stop behavior provides an indirect indication of potential NVH and drivability implications. These results suggest that the proposed calibration method can improve fuel economy while providing a preliminary assessment of SOC balance and engine operating characteristics. Nevertheless, comprehensive multi-objective optimization and experimental validation of NVH and drivability remain necessary for practical engineering applications.

3.4. Hardware-in-the-Loop Validation

The Hardware-in-the-Loop (HIL) platform established for supplementary validation is shown in Figure 14. The platform mainly consists of a dSPACE/simulator(made in Germany), a RapidECU-U2 controller(made in China), a low-voltage DC power supply, and a host computer. The dSPACE/simulator and the RapidECU-U2 controller are respectively monitored, measured, and calibrated through the ControlDesk(4.0) and MeCa(2.0) software installed on the host computer. The low-voltage DC power supply provides a 24 V DC voltage for the vehicle controller, and real-time communication between the dSPACE/simulator and the RapidECU-U2 controller is realized through the CAN bus.

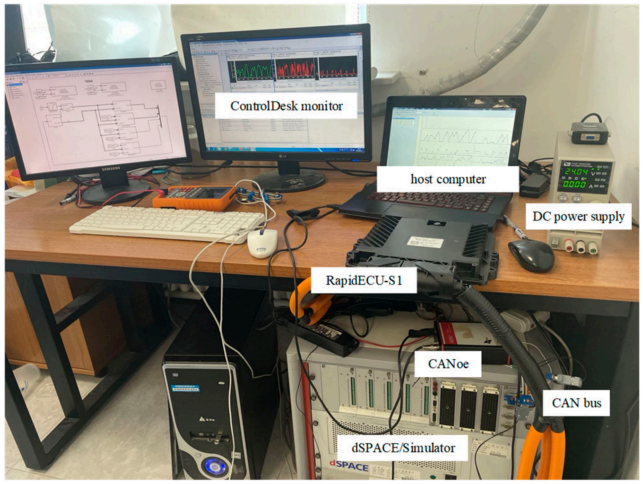


Figure 14. Hardware-in-the-loop (HIL) test platform.

To provide supplementary validation beyond offline simulation, HIL tests were conducted under the CCBC driving cycle. In this validation, the optimized VCU calibration parameters obtained from the proposed method were implemented in the RapidECU-U2 controller, while the plant model of the hybrid electric vehicle was executed in real time on the dSPACE platform. The vehicle speed tracking, battery SOC trajectory, and engine operating state obtained from the HIL tests were then compared with the corresponding simulation results.

The comparison results are shown in Figure 15. It can be seen that the HIL results agree well with the simulation results in terms of velocity tracking, SOC evolution, and engine operating-state transitions under the CCBC driving cycle. In particular, the vehicle speed follows the target cycle accurately, the SOC variation trend remains consistent, and the engine on/off operating characteristics are reproduced with satisfactory consistency. These results indicate that the optimized VCU calibration parameters can be implemented in real time and that the proposed calibration framework has good engineering feasibility under the investigated cycle. To further quantify the consistency between simulation and HIL, the key indicators under the CCBC are summarized in Table 8. The comparison shows that the differences in the main response variables remain within an acceptable range, further supporting the real-time feasibility of the optimized calibration parameters.

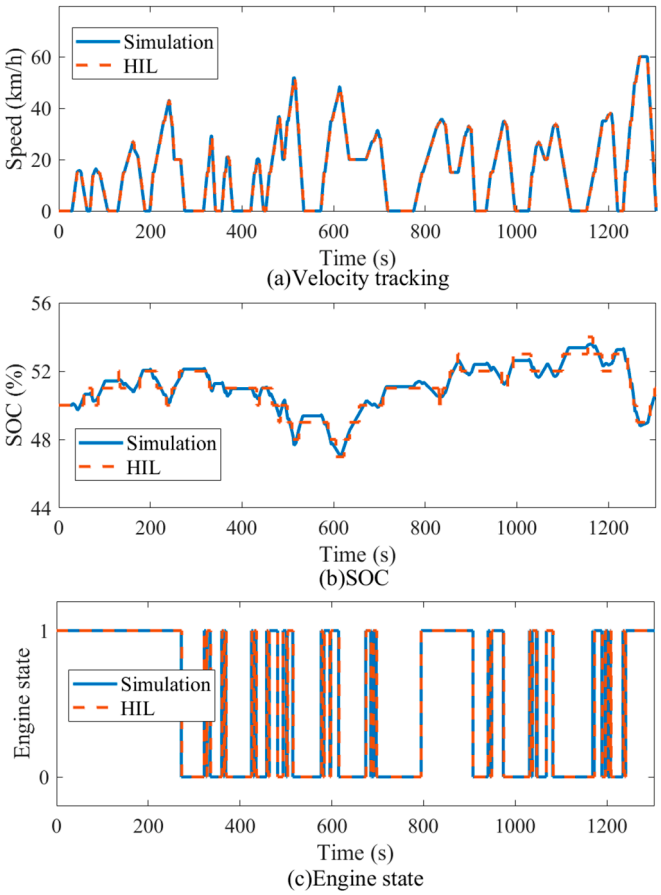


Figure 15. Comparison of simulation and HIL results under the CCBC driving cycle.

Table 8. Quantitative comparison of simulation and HIL results.

Metric (Unit)	Simulation	HIL Test	Difference
$f_{e,u}$ (L/100 km)	15.97	16.09	0.12
Final SOC (%)	50.6	51	0.4

However, slight discrepancies are still observable, which are typical for real-time HIL implementations. For instance, a minor time lag can be observed in the engine start-stop transitions (Figure 15c) because the actual VCU requires a certain execution cycle and the CAN bus communication introduces latency compared with the purely mathematical simulation. In addition, the HIL velocity is typically processed with a 1 km/h discretization due to sensor resolution and signal sampling limitations, which leads to a slight staircase effect and minor tracking deviations. As a result of these hardware and communication constraints, the HIL test exhibits a marginally higher equivalent fuel consumption and a slightly different final SOC.

It should be noted that the present HIL validation is intended to verify the real-time implementation feasibility and response consistency of the proposed calibration method, rather than to serve as full vehicle-level experimental confirmation of the absolute fuel-economy improvement. Nevertheless, the supplementary HIL results provide additional support for the rationality and applicability of the proposed VCU calibration framework.

4. Discussion

The proposed optimization-based VCU calibration design method for planetary power-split hybrid electric systems has demonstrated its effectiveness in the calibration of VCU control parameters for planetary power-split hybrid electric vehicles. Compared with conventional calibration approaches that rely heavily on empirical trial and error, the proposed method begins with the control strategy and integrates feasible-range determination, system response analysis, and numerical optimization into a systematic parameter calibration procedure. Furthermore, the supplementary HIL validation under the CCBC driving cycle provides additional evidence of the real-time implementation feasibility and response consistency of the optimized calibration parameters. Nevertheless, the present validation is still limited to simulation and HIL testing under the investigated cycle, and full vehicle-level experimental validation remains necessary in future work. The proposed method therefore provides a useful basis for further engineering application and subsequent experimental verification.

The local sensitivity analysis revealed the independent effects of the calibration parameters on vehicle-level combined fuel consumption. The results show that the power demand threshold has a pronounced influence on combined fuel consumption within its feasible range, with fuel consumption increasing as the threshold increases. A lower power demand threshold causes the engine to be activated at a lower level of vehicle power demand, thereby narrowing the power range of all-electric operation and increasing the participation of hybrid driving. Under the rule-based engine optimal operating strategy, this adjustment can improve the coordination between engine operation and battery power utilization, thereby reducing combined fuel consumption. The effect of the SOC threshold on combined fuel consumption exhibits a distinct piecewise characteristic. When the SOC threshold is lower than the minimum SOC reached during the driving cycle, variations in this parameter do not trigger operating-mode transitions, and fuel consumption therefore remains essentially unchanged. Once the SOC threshold exceeds this critical value, the system enters hybrid driving mode earlier because of the SOC constraint, resulting in an increase in combined fuel consumption. By comparison, the charging coefficient has only a limited effect on the fuel-consumption response under the current initial parameter settings and driving-cycle conditions. This is mainly because the battery SOC remains above the corresponding charging-control boundary throughout the simulation, preventing the engine-driven charging process from being effectively activated. These results demonstrate that local sensitivity analysis can intuitively reveal the influence of an individual calibration parameter on the system response and provide a preliminary basis for screening the key calibration parameters.

Global sensitivity analysis further overcomes the limitation of local sensitivity analysis, which can capture only the independent effect of a single parameter. In this study, 200 sample points were generated within the feasible parameter space using an optimal Latin hypercube design, providing favorable space-filling characteristics and representativeness. Pareto analysis was then employed to quantitatively evaluate the contributions of the individual calibration parameters and their interaction terms to the vehicle's combined fuel consumption. The results indicate that the power demand threshold and SOC threshold are the dominant factors affecting combined fuel consumption, with their contributions being substantially greater than that of the charging coefficient. This finding demonstrates that, under the current control strategy, these two parameters exert more direct effects on the operating-mode transition boundaries and vehicle-level energy allocation.

To further verify the rationality of the key calibration parameter screening results, Figure 16 presents scatter plots illustrating the relationships between the power demand threshold, SOC threshold, and combined fuel consumption. As shown in the left subplot

of Figure 16, the power demand threshold exhibits a clear positive relationship with combined fuel consumption, with a regression slope of approximately 0.035. This relationship indicates that lowering the power demand threshold advances engine activation under power-demand-based transition conditions. Under the rule-based strategy for optimal engine operation, earlier engine engagement improves the coordination between engine efficiency and battery power utilization, thereby reducing the combined fuel consumption. The right subplot of Figure 16 shows that the effect of the SOC threshold on fuel consumption exhibits a distinct piecewise characteristic. When the SOC threshold is below 78%, its variation has only a limited effect on combined fuel consumption. Once the threshold exceeds 78%, however, the combined fuel consumption increases with the SOC threshold. This trend is highly consistent with the piecewise influence of the SOC threshold identified through the local sensitivity analysis. The combined results of the Pareto analysis and scatter-plot correlation analysis confirm that selecting the power demand threshold and SOC threshold as the key calibration parameters for the subsequent optimization is well justified. Meanwhile, temporarily excluding the charging coefficient from the optimization variables effectively reduces the dimensionality of the optimization problem, as well as the associated computational cost and calibration workload.

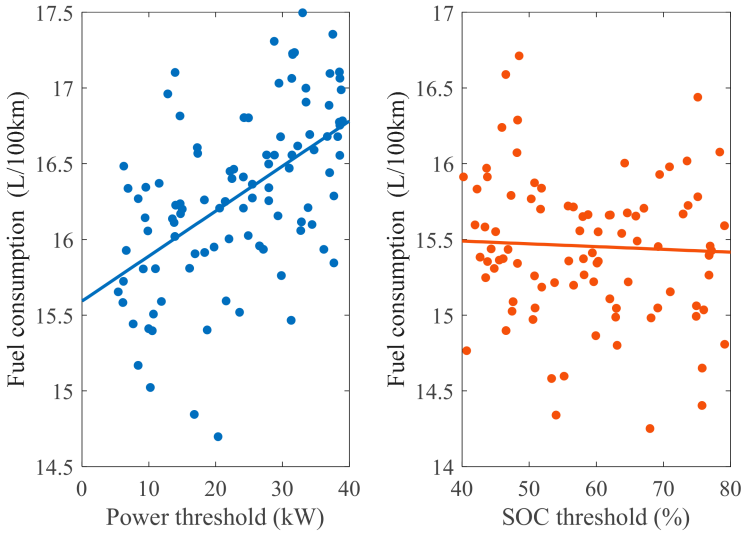


Figure 16. Scatter plots of key calibration parameters versus combined fuel consumption.

After global optimization, the SOC threshold was reduced from 72% to 55%, while the power demand threshold decreased from 27 kW to 7 kW. The resulting reduction in theoretical combined fuel consumption reflects the overall effect of jointly adjusting these two calibration parameters. Unlike the local sensitivity analysis, which evaluates individual parameter effects under fixed baseline conditions, the optimization process considers simultaneous parameter variations and their potential interactions. Consequently, the SOC trajectory and the corresponding operating-mode transition conditions may differ from those observed under the initial parameter combination. The optimization results therefore demonstrate the effectiveness of the combined parameter calibration strategy rather than the isolated effect of either parameter.

Consequently, the theoretical combined fuel consumption per 100 km decreased from 16.71 L/100 km to 15.97 L/100 km, corresponding to a reduction of 4.43%. The two optimized thresholds have different effects on operating-mode transitions. The lower SOC threshold delays SOC-triggered engine activation and permits deeper utilization of battery energy, whereas the lower power demand threshold advances power-demand-triggered engine activation and increases hybrid-mode participation under medium- and high-load

conditions. Extending pure electric operation may reduce fuel consumption under certain low-speed and low-load conditions by avoiding inefficient engine operation. However, a higher proportion of pure electric driving does not necessarily lead to lower SOC-corrected combined fuel consumption, since battery energy depletion and subsequent energy replenishment must also be considered. As indicated by the main-effect results in Figure 7a, increasing the power demand threshold tends to increase the theoretical combined fuel consumption under the investigated conditions, suggesting that an appropriate balance between pure electric and hybrid operation is more beneficial than simply maximizing the duration of pure electric driving. Their coordinated adjustment improves the balance between battery energy utilization and efficient engine operation. In addition, the optimized engine operating points become more concentrated in the high-efficiency region, indicating that the parameter optimization improves both the operating-mode transition boundaries and the utilization of the engine high-efficiency region. It should be noted that operating the engine and motor-generators near their respective high-efficiency regions is beneficial for reducing energy losses, but the optimal operating points of individual components do not necessarily correspond to the minimum overall vehicle fuel consumption. Therefore, further improvements may be achieved by considering the combined effects of engine fuel efficiency, motor-generator conversion efficiency, and battery charging and discharging efficiency within the system-level energy management framework. The adaptive simulated annealing algorithm converged steadily after the 133rd iteration, demonstrating favorable global search capability and convergence stability in solving nonlinear and multimodal VCU parameter optimization problems.

Previous studies have demonstrated the effectiveness of optimization-based methods in improving the calibration and control performance of hybrid powertrains [17,18]. These findings are consistent with the results of the present study, which further demonstrate that systematic parameter screening and coordinated optimization can improve the fuel economy of planetary power-split hybrid electric vehicles. Related investigations have also confirmed the potential of automated calibration and optimization techniques in different powertrain control applications [19–22]. Compared with these studies, the present work focuses on the systematic screening and optimization of VCU parameters in a planetary power-split hybrid electric system. By integrating local sensitivity analysis, DOE-based global sensitivity analysis, and adaptive simulated annealing, the proposed method identifies the dominant calibration parameters and their interaction effects before optimization. The optimized parameter combination reduces the theoretical combined fuel consumption from 16.71 L/100 km to 15.97 L/100 km, corresponding to a reduction of 4.43%. This result indicates that the proposed calibration procedure can effectively improve fuel economy through systematic parameter identification and coordinated optimization. It also highlights the importance of considering parameter interactions when calibrating complex hybrid powertrain control systems.

Although the proposed VCU parameter optimization and calibration method has achieved a certain reduction in theoretical combined fuel consumption per 100 km, several aspects warrant further investigation. (1) Although the theoretical fuel consumption model is supported by previous research, the present VCU calibration framework is primarily evaluated through simulation under the CCBC conditions. Therefore, the reported 4.43% reduction represents a theoretical improvement under the adopted modeling assumptions rather than an experimentally confirmed fuel-saving benefit. The HIL results provide additional evidence of real-time implementation feasibility and response consistency. Further vehicle-level experiments under diverse operating conditions are therefore necessary to verify the actual fuel-saving benefits and robustness of the proposed calibration method. Future studies may incorporate different vehicle platforms, various initial SOC conditions, and

a broader range of representative operating conditions, including urban, suburban, highway, grade, and low-temperature driving. The sensitivity characteristics of the key calibration parameters and the corresponding optimization results can then be further evaluated to assess the applicability, robustness, and stability of the proposed method across different vehicle types and operating conditions. (2) Theoretical combined fuel consumption per 100 km is adopted as the primary system response in this study, with emphasis placed on the influence of control parameter variations on vehicle fuel economy. However, VCU parameter calibration also involves comprehensive performance requirements related to dynamic response, SOC balance, operating-mode transition smoothness, battery lifetime, and emissions. Future research may therefore introduce additional evaluation metrics, such as SOC deviation, engine start–stop frequency, operating-mode transition shock, battery charging and discharging loads, and emission indices. On this basis, a multi-objective optimization-based calibration model can be established to achieve coordinated improvements in fuel economy, dynamic performance, driving smoothness, and system durability. (3) The screening and optimization of the key calibration parameters in this study are mainly conducted through offline simulation under prescribed driving-cycle conditions. This approach provides a relatively consistent evaluation basis for analyzing the effects of different VCU parameter combinations on vehicle-level energy allocation and fuel consumption. However, actual driving and traffic conditions may introduce additional variations in vehicle operating demands. For example, aggressive acceleration and frequent stop-and-go operations can change instantaneous power demand and operating-mode transition frequency, while traffic congestion may affect average vehicle speed and regenerative braking opportunities. Road gradients and vehicle load variations can also change the required traction power and engine operating-point distribution. These factors may consequently influence the sensitivity characteristics and optimal values of VCU calibration parameters. Therefore, the optimization results obtained in this study should be interpreted within the scope of the adopted simulation conditions. Future work will further investigate the effects of different driving behaviors, traffic conditions, road gradients, and vehicle loads on VCU calibration performance, and evaluate the adaptability of the proposed method under more diverse operating conditions. Furthermore, incorporating predicted driving conditions into condition-dependent energy management strategies may further improve fuel economy under varying operating conditions. Future work will explore the integration of driving-condition prediction and adaptive energy management with the proposed VCU calibration framework, together with a comparative evaluation of two-speed AMT operating conditions, to further assess its adaptability and energy-saving potential.

5. Conclusions

This study investigates a planetary power-split hybrid electric vehicle and develops an optimization-based VCU parameter calibration method that integrates sensitivity analysis with an adaptive simulated annealing algorithm, based on the power-split powertrain architecture and a rule-based engine optimal operating strategy. First, according to the operating-mode transition logic and power allocation relationships of the energy management strategy, the SOC threshold, power demand threshold, and charging coefficient are selected as the initial calibration parameters. Their feasible ranges are then determined by considering the allowable battery SOC range, vehicle power demand distribution, and SOC balance constraints. Subsequently, theoretical combined fuel consumption per 100 km is adopted as the system response. Local sensitivity analysis is performed to identify the independent influence of each parameter on fuel consumption, while an optimal Latin hypercube design and Pareto analysis are employed to further quantify the contributions of multiple parameters and their interaction terms to the fuel-consumption response. Finally,

the adaptive simulated annealing algorithm is applied to perform global optimization of the identified key calibration parameters.

The results indicate that the power demand threshold has a significant positive effect on combined fuel consumption. A lower power demand threshold advances power-demand-triggered engine activation, narrows the power range of all-electric operation, and increases hybrid-mode participation. Under the rule-based strategy for optimal engine operation, this adjustment improves the coordination between engine efficiency and battery power utilization, thereby reducing combined fuel consumption. The effect of the SOC threshold exhibits a distinct piecewise characteristic. When the SOC threshold exceeds approximately 78%, it significantly alters the operating-mode transition boundary and leads to increased fuel consumption. By contrast, the charging coefficient exhibits relatively low sensitivity under the current initial SOC condition and driving cycle. The global sensitivity analysis further demonstrates that the SOC threshold, power demand threshold, and their associated quadratic and interaction terms are the primary factors affecting the theoretical combined fuel consumption. This finding indicates that vehicle fuel economy is governed not only by individual threshold parameters but also by the coupling effects among these parameters. After optimization using the adaptive simulated annealing algorithm, the SOC threshold was adjusted from 72% to 55%, while the power demand threshold was reduced from 27 kW to 7 kW. Consequently, the theoretical combined fuel consumption per 100 km decreased from 16.71 L/100 km to 15.97 L/100 km, corresponding to a reduction of 4.43%. These results demonstrate that the proposed method can effectively identify the key calibration parameters and determine a favorable parameter combination, thereby providing a useful reference for VCU parameter calibration and the optimization of energy-efficient control strategies for planetary power-split hybrid electric systems.

Author Contributions: Conceptualization, J.Q. and Y.X.; methodology, J.Q.; software, J.H.; validation, J.Q.; formal analysis, L.Z.; investigation, L.Z.; resources, Y.X.; data curation, J.Q.; writing—original draft preparation, J.Q.; writing—review and editing, Y.X., Y.Z. and Z.W.; visualization, Z.W.; supervision, Z.W.; project administration, Y.X.; funding acquisition, Y.X. All authors have read and agreed to the published version of the manuscript.

Funding: This research was funded by the Zhongyuan Leading Talent Program (Science and Technology Innovation), grant number 264200510036, and the Key Scientific Research Projects of Higher Education Institutions in Henan Province, grant number 25CY041.

Data Availability Statement: The original contributions presented in this study are included in the article. Further inquiries can be directed to the corresponding author.

Conflicts of Interest: The authors declare no conflicts of interest.

Abbreviations

The following abbreviations are used in this manuscript:

VCU	Vehicle Control Unit
SOC	State of Charge
SA	Simulated Annealing
Opt LHD	Optimal Latin Hypercube Design
MG	Motor Generator
LHD	Latin Hypercube Design
HEV	Hybrid Electric Vehicle
EMS	Energy Management Strategy
DOE	Design of Experiments
ASA	Adaptive Simulated Annealing

References

1. Zhang, F.; Wang, L.; Coskun, S.; Pang, H.; Cui, Y.; Xi, J. Energy management strategies for hybrid electric vehicles: Review, classification, comparison, and outlook. *Energies* **2020**, *13*, 3352. [CrossRef]
2. Cao, Y.; Ming, Y.; Sun, X. An overview of modelling and energy management strategies for hybrid electric vehicles. *Appl. Sci.* **2023**, *13*, 5947. [CrossRef]
3. Yu, J.; Zhang, X.; Yan, H.; Li, X. Multi-objective virtual calibration method for parameters in two control strategies of a complex hybrid electric vehicle. *Eng. Appl. Artif. Intell.* **2025**, *159*, 111669. [CrossRef]
4. Wang, H.; Chang, C.; Pan, Z.; Zhai, X.; Liu, H.; Zhang, S.; Liu, Y. Optimization of energy management strategies for multi-mode hybrid electric vehicles driven by travelling road condition data. *Sci. Rep.* **2025**, *15*, 12684. [CrossRef] [PubMed]
5. Feng, R.; Li, G.; Zhao, Z.; Deng, B.; Hu, X.; Liu, J.; Wang, S. Control strategy optimization of hybrid electric vehicle for fuel saving based on energy flow experiment and simulation. *J. Clean. Prod.* **2023**, *420*, 138344. [CrossRef]
6. Guo, N.; Zhang, X.; Zou, Y.; Du, G.; Wang, C.; Guo, L. Predictive energy management of plug-in hybrid electric vehicles by real-time optimization and data-driven calibration. *IEEE Trans. Veh. Technol.* **2021**, *71*, 5677–5691. [CrossRef]
7. Peng, J.; Zhang, H.; Ma, C.; He, H. Powertrain Parameters' Optimization for a Series–Parallel Plug-In Hybrid Electric Bus by Using a Combinatorial Optimization Algorithm. *IEEE J. Emerg. Sel. Top. Power Electron.* **2023**, *11*, 32–43. [CrossRef]
8. Schmidt, H.; Büttner, K.; Prokop, G. Methods for Virtual Validation of Automotive Powertrain Systems in Terms of Vehicle Drivability—A Systematic Literature Review. *IEEE Access* **2023**, *11*, 27043–27065. [CrossRef]
9. Pan, W.; Wu, Y.; Tong, Y.; Li, J.; Liu, Y. Optimal rule extraction-based real-time energy management strategy for series-parallel hybrid electric vehicles. *Energy Convers. Manag.* **2023**, *293*, 117474. [CrossRef]
10. Yang, C.; Wang, X.; Zhao, J.; He, L. Optimization of the energy management system in hybrid electric vehicles considering cabin temperature. *Appl. Therm. Eng.* **2024**, *242*, 122504. [CrossRef]
11. Xiao, R.; Liang, D.; Ba, T.; Sun, M.; Chen, G.; Yao, G.; Zheng, Y. Integrated optimization of dedicated engine and energy management strategy for the plug-in hybrid commercial vehicle at high altitude. *Energy* **2024**, *290*, 130253. [CrossRef]
12. Zhang, B.; Chang, L.; Teng, T.; Chen, Q.; Li, Q.; Cao, Y.; Yang, S.; Zhang, X. Multi-objective optimization with Q-learning for cruise and power allocation control parameters of connected fuel cell hybrid vehicles. *Appl. Energy* **2024**, *373*, 123910. [CrossRef]
13. Geng, W.; Lou, D.; Wang, C.; Zhang, T. A cascaded energy management optimization method of multimode power-split hybrid electric vehicles. *Energy* **2020**, *199*, 117224. [CrossRef]
14. Lin, X.; Zeng, S.; Li, X. Online correction predictive energy management strategy using the Q-learning based swarm optimization with fuzzy neural network. *Energy* **2021**, *223*, 120071. [CrossRef]
15. Anselma, P.; Marco, D.; Giovanni, B. Battery high temperature sensitive optimization-based calibration of energy and thermal management for a parallel-through-the-road plug-in hybrid electric vehicle. *Appl. Sci.* **2021**, *11*, 8593. [CrossRef]
16. Ferrara, A.; Zendegan, S.; Koegeler, H.-M.; Gopi, S.; Huber, M.; Pell, J.; Hametner, C. Optimal calibration of an adaptive and predictive energy management strategy for fuel cell electric trucks. *Energies* **2022**, *15*, 2394. [CrossRef]
17. Du, W.; Zhao, S.; Jin, L.; Gao, J.; Li, H. Parameter optimization of rule-based control strategy for multi-mode hybrid electric vehicle. *Proc. Inst. Mech. Eng. Part D J. Automob. Eng.* **2020**, *234*, 2706–2716. [CrossRef]
18. Düzgün, M.T.; Dorscheidt, F.; Krysmon, S.; Bailly, P.; Lee, S.-Y.; Dönitz, C.; Pischinger, S. Virtual multi-criterial calibration of operating strategies for hybrid-electric powertrains. *Vehicles* **2023**, *5*, 1367–1383. [CrossRef]
19. Mishra, K.; Guy, C.; Krishnaswamy, S. Automated calibration of gearshift controllers using iterative learning control for hybrid systems. *Control Eng. Pract.* **2021**, *111*, 104786. [CrossRef]
20. Lee, H.; Gu, B.; Cha, S.W.; Lim, W. Model based automated calibration for shift control of automatic transmission. *Int. J. Automot. Technol.* **2021**, *22*, 269–280. [CrossRef]
21. Garg, P.; Emilia, S.; Frank, W. Systematic hyperparameter selection in Machine Learning-based engine control to minimize calibration effort. *Control Eng. Pract.* **2023**, *140*, 105666. [CrossRef]
22. Ritzmann, J.; Chinellato, O.; Hutter, R.; Onder, C. Optimal integrated emission management through variable engine calibration. *Energies* **2021**, *14*, 7606. [CrossRef]
23. Huang, K.D.; Nguyen, M.K.; Chen, P.T. A rule-based control strategy of driver demand to enhance energy efficiency of hybrid electric vehicles. *Appl. Sci.* **2022**, *12*, 8507. [CrossRef]
24. Zou, S.; Zhang, J.; Yang, Y.; Zhou, Y.; Liu, Y.; Peng, J.; Feng, X. Rule-based control strategy for a novel dual-motor PHEV improved by dynamic programming. *Electronics* **2025**, *14*, 1450. [CrossRef]
25. Ba, T.; Gao, Y.; Wang, Q.; Zeng, X.; Song, D. Optimization of control strategy for a parallel hybrid electric bus based on dynamic programming algorithm. *Automot. Eng.* **2015**, *37*, 1359–1365.
26. Zeng, X.; Qian, Q.; Chen, H. A Unified Quantitative Analysis of Fuel Economy for Hybrid Electric Vehicles Based on Energy Flow. *J. Clean. Prod.* **2021**, *292*, 126040. [CrossRef]

27. Lian, Y.; Zhao, B.; Du, W.; Zeng, D.; Li, S.; Wang, P. Predictive energy management of series-parallel hybrid electric vehicles and its sensitivity analysis to dynamic traffic environment. *Proc. Inst. Mech. Eng. Part D J. Automob. Eng.* **2026**, *240*, 2054–2067. [CrossRef]
28. Li, M.; Yu, P.; Wang, Y.; Sun, Z.; Chen, Z. Topology comparison and sensitivity analysis of fuel cell hybrid systems for electric vehicles. *IEEE Trans. Transp. Electrif.* **2022**, *9*, 5111–5121. [CrossRef]
29. Guo, N.; Zhang, W.; Li, J.; Chen, Z.; Li, J.; Sun, C. Predictive energy management of fuel cell plug-in hybrid electric vehicles: A co-state boundaries-oriented PMP optimization approach. *Appl. Energy* **2024**, *362*, 122882. [CrossRef]
30. Qin, C.; Jin, Y.; Tian, M.; Ju, P.; Zhou, S. Comparative study of global sensitivity analysis and local sensitivity analysis in power system parameter identification. *Energies* **2023**, *16*, 5915. [CrossRef]

Disclaimer/Publisher's Note: The statements, opinions and data contained in all publications are solely those of the individual author(s) and contributor(s) and not of MDPI and/or the editor(s). MDPI and/or the editor(s) disclaim responsibility for any injury to people or property resulting from any ideas, methods, instructions or products referred to in the content.